Anomalies in the strength of the Hadley cells are inversely correlated with anomalies in the strength of the Walker oscillation (*18*, *31*): Weakened Hadley cells correlate with episodes of La Niña and strong Walker circulation. Second, the stronger oceanic heat flux to the high latitudes is consistent with enhanced Ekman flow of warm water poleward as a result of increased Walker circulation. The constraint of a balanced heat budget during the Pliocene implies that this increased heat loss at high latitudes through vigorous deep-ocean thermohaline circulation is accompanied by a shoaling of the tropical thermocline (*32*). Most oceanic heat gain occurs in low and mid-latitude upwelling zones and is large (small) when the thermocline is shallow (deep). During the Pliocene, the deeper thermocline in the WEP argues that thermocline tilt must be greater to allow shoaling of the EEP thermocline.

Our data rebut the hypothesis that "hothouse" climates collapse onto an El Niño–like state, in agreement with Eocene hothouse studies (*33*), and indicate that the tropical upper-ocean structure during the warm Pliocene was indicative of a La Niña–like state consistent with the dynamical "ocean thermostat." Twentieth-century global warming has also resulted in a stronger east-west SST gradient (*34*) on a contrastingly rapid time scale. Both of these scenarios, reflecting mean and transient Pacific states, respectively, support the role of the Bjerknes feedback inhibiting an El Niño positive feedback to global warming. Interestingly, during the Pliocene the increase in east-west SST gradient is due to eastern cooling, whereas during the 20th century it is due to WEP warming. In the near future, if the warming of the WEP warm pool reaches a limit without a compensating cooling in the east (afforded by the EUC during the Pliocene), could the Bjerknes feedback be reversed to incite accelerated warmth of an El Niño–like state?

References and Notes

1. W. J. Cai, P. H. Whetton, *Geophys. Res. Lett.* **27**, 2577 (2000).
2. K. E. Trenberth, D. P. Stepaniak, J. M. Caron, *J. Geophys. Res.* **107**, 4066 (2002); 10.1029/2000JD000297.
3. Here, we use "hothouse" to denote the warm early-mid Pliocene climate regime when the Northern Hemisphere lacked substantial ice sheets, and "icehouse" for the Middle to Late Pleistocene regime characterized by the waxing and waning of major Northern Hemisphere ice sheets.
4. M. Budyko, Y. A. Izrael, Eds., *Anthropogenic Climate Changes* (L. Gidrometeoizdat, Leningrad, 1987).
5. T. C. Crowley, *Quat. Sci. Rev.* **10**, 275 (1991).
6. M. E. Raymo, B. Grant, M. Horowitz, G. H. Rau, *Mar. Micropaleontol.* **27**, 313 (1996).
7. Global climate is influenced by the seesaw of the tropical Pacific thermocline tilt, or ENSO. This connection underpins the proposal of persistent El Niño conditions during geological "hothouse periods." The natural mode of oscillation is attributable to ocean-atmosphere interactions in which the trade winds create SST gradients that in turn reinforce the winds. In the Pacific, the prevailing easterly trade winds blow warm surface waters along the equator, creating a deep warm pool toward the western Pacific margin (*35*). This causes the tropical Pacific thermocline to become deeper in the west than in the east. Water is returned, along the thermocline, in the EUC, to the east, where it upwells. The zonal SST gradient between the west and east Pacific drives an east-west atmospheric circulation (the Walker Cell). This circulation further increases upwelling in the east Pacific, a process known as the Bjerknes feedback (*36*). Warm El Niño events occur when easterly trade winds decrease or reverse direction and warm water from the west Pacific spreads eastwards and, in doing so, reduces the Pacific thermocline tilt. This decreases the zonal temperature gradient, causing a breakdown of Walker Cell circulation. Cold La Niña events occur when trade winds are strong and induce a steep thermocline tilt. Changes in atmospheric circulation above the tropical Pacific cause changes in teleconnections to higher latitudes, with global climatic consequences on an interannual time scale. For this study, in which we investigate the average condition of the low-latitude ocean on million-year time scales, we refer to an El Niño (La Niña)–like state to reflect reduced (increased) east-west SST gradient, reduced (increased) thermocline tilt, and deeper (shallower) thermocline in the EEP. The detailed spatial patterns of atmosphere and ocean conditions associated with these two proposed states on geological time scales are currently unknown and may be very different from interannual configurations (*37*).
8. W. P. Chaisson, A. C. Ravelo, *Paleoceanography* **15**, 497 (2000).
9. M. A. Cane, P. Molnar, *Nature* **411**, 157 (2001).
10. P. Molnar, M. A. Cane, *Paleoceanography* **17**, 663 (2002); 10.1029/2001PA000663.
11. K. G. Cannariato, A. C. Ravelo, *Paleoceanography* **12**, 805 (1997).
12. Materials and methods are available as supporting material on *Science* Online.
13. At the critical site for our new interpretation, site 847, carbonate accumulation rates were higher prior to 4 Ma, which implies that preservation was improved during the Pliocene relative to today (*17*). The chemistry of *G. sacculifer* is insensitive to dissolution due to chemical homogeneity throughout the test (*38*). Planktonic Sr/Ca is a potential indicator of dissolution. Further evidence of the minimal influence of dissolution on these records is the covariation of Sr/Ca of *G. sacculifer* and *G. tumida* from both sites (Fig. 1E), which also parallels oceanic Sr/Ca evolution (*39*).
14. S. G. Philander, A. V. Federov, *Paleoceanography* **18**, 837 (2003); 10.1029/2002PA000837.
15. T. Izumo, J. Picaut, B. Blanke, *Geophys. Res. Lett.* **29**, 15073 (2002); 10.1029/2002GL015073.
16. S. A. Hovan, *Proc. ODP Sci. Results* **138**, 615 (1995).
17. T. King, *Mar. Micropaleontol.* **27**, 63 (1996).
18. A. C. Clement, R. Seager, M. A. Cane, S. E. Zebiak, *J. Clim.* **9**, 2190 (1996).
19. M. A. Cane *et al.*, *Science* **275**, 957 (1997).
20. K. B. Rodgers, M. A. Cane, N. H. Naik, D. P. Schrag, *J. Geophys. Res.* **104**, 20,551 (1999).
21. D. Gu, S. G. H. Philander, *Science* **275**, 805 (1997).
22. E. J. Rohling, *Mar. Geol.* **163**, 1 (2000).
23. C. H. Lear, Y. Rosenthal, J. D. Wright, *Earth Planet. Sci. Lett.* **210**, 425 (2003).
24. Y. Rosenthal, G. P. Lohmann, K. C. Lohmann, R. M. Sherrell, *Paleoceanography* **15**, 135 (2000).
25. H. J. Spero, K. M. Mielke, E. M. Kalve, D. W. Lea, D. K. Pak, *Paleoceanography* **18**, 1022 (2003); 10.1029/2002PA000814.
26. G. A. Schmidt, *Paleoceanography* **14**, 422 (1999).
27. L. C. Sloan, T. J. Crowley, D. Pollard, *Mar. Micropaleontol.* **27**, 51 (1996).
28. K. B. Rodgers *et al.*, *Geophys. Res. Lett.* **30**, 16003 (2003); 10.1029/2002GL016003.
29. K. B. Rodgers, M. Latif, S. Legutke, *Geophys. Res. Lett.* **27**, 2941 (2000).
30. K. Billups, A. C. Ravelo, J. C. Zachos, *Paleoceanography* **13**, 84 (1998).
31. A. H. Oort, J. J. Yienger, *J. Clim.* **9**, 2751 (1996).
32. G. Boccaletti, R. C. Pacanowski, S. G. H. Philander, A. V. Federov, *J. Phys. Oceangr.* **34**, 888 (2004).
33. M. Huber, R. Caballero, *Science* **299**, 877 (2003).
34. M. A. Cane, *Earth Planet. Sci. Lett.* **164**, 1 (2004).
35. E. Maier-Reimer, U. Mikalojewicz, T. J. Crowley, *Paleoceanography* **5**, 349 (1990).
36. A. V. Federov, G. Philander, *Science* **288**, 1997 (2000).
37. W. Hazeleger, R. Seager, M. A. Cane, N. H. Naik, *J. Phys. Oceanogr.* **34**, 320 (2004).
38. S. Brown, H. Elderfield, *Paleoceanography* **11**, 543 (1996).
39. C. H. Lear, H. Elderfield, P. A. Wilson, *Earth Planet. Sci. Lett.* **208**, 69 (2003).
40. P. Anand, H. Elderfield, M. H. Conte, *Paleoceanography* **18**, 846 (2003); 10.1029/2002PA000846.
41. S. Levitus, T. Boyer, *World Ocean Atlas 1994*, *Vol. 4*, NOAA National Environmental and Satellite Data and Information Service, U.S. Department of Commerce, Washington, DC (1994).
42. D. W. Lea, D. K. Pak, H. J. Spero, *Science* **289**, 1719 (2000).
43. E. C. Farmer, Thesis, Columbia University (2000).

44. We thank M. Evans and M. Cane for invaluable exchange of ideas, two anonymous reviewers who greatly improved this manuscript, J. Arden for technical support, and D. Sansom for art support. Further thanks to the Ocean Drilling Program for providing samples and to the Natural Environment Research Council for providing financial support.

Supporting Online Material

www.sciencemag.org/cgi/content/full/307/5717/1948/DC1
Materials and Methods
References

30 August 2004; accepted 24 January 2005
10.1126/science.1104666

Soft-Tissue Vessels and Cellular Preservation in *Tyrannosaurus rex*

Mary H. Schweitzer,[1,2,3]* Jennifer L. Wittmeyer,[1] John R. Horner,[3] Jan K. Toporski[4]†

Soft tissues are preserved within hindlimb elements of *Tyrannosaurus rex* (Museum of the Rockies specimen 1125). Removal of the mineral phase reveals transparent, flexible, hollow blood vessels containing small round microstructures that can be expressed from the vessels into solution. Some regions of the demineralized bone matrix are highly fibrous, and the matrix possesses elasticity and resilience. Three populations of microstructures have cell-like morphology. Thus, some dinosaurian soft tissues may retain some of their original flexibility, elasticity, and resilience.

A newly discovered specimen of *Tyrannosaurus rex* [Museum of the Rockies (MOR) specimen 1125] was found at the base of the Hell Creek Formation, 8 m above the Fox Hills Sandstone, as an association of disarticulated elements. The specimen was incorpo-

rated within a soft, well-sorted sandstone that was interpreted as estuarine in origin. Although some bones are slightly deformed or crushed, preservation is excellent. MOR 1125 represents a relatively small individual of *T. rex,* with a femoral length of 107 cm, as compared to the Field Museum (Chicago) specimen (FMNH PR2081) that has a femoral length of approximately 131 cm. On the basis of calculated lines of arrested growth (LAG), we estimated that this animal was 18 ± 2 years old at death (*1*).

No preservatives were applied to interior fragments of the femur of MOR 1125 during preparation, and these fragments were reserved for chemical analyses. In addition to the dense compact bone typical of theropods, this specimen contained regions of unusual bone tissue on the endosteal surface (*2*). Cortical and endosteal bone tissues were demineralized (*3*), and

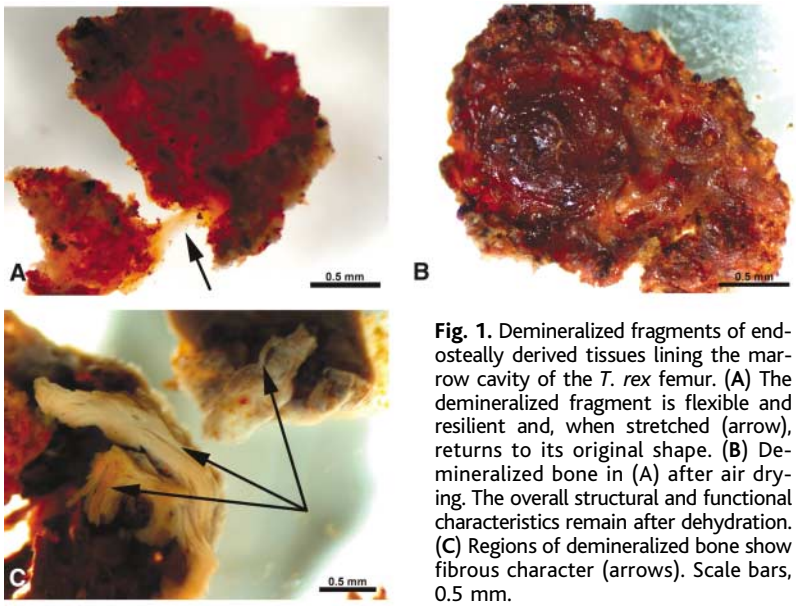

Fig. 1. Demineralized fragments of endosteally derived tissues lining the marrow cavity of the *T. rex* femur. (**A**) The demineralized fragment is flexible and resilient and, when stretched (arrow), returns to its original shape. (**B**) Demineralized bone in (A) after air drying. The overall structural and functional characteristics remain after dehydration. (**C**) Regions of demineralized bone show fibrous character (arrows). Scale bars, 0.5 mm.

[1]Department of Marine, Earth, Atmospheric Sciences, North Carolina State University, Raleigh, NC 27695, USA. [2]North Carolina State Museum of Natural Sciences, Raleigh, NC 27601, USA. [3]Museum of the Rockies, Montana State University, Bozeman, MT 59717, USA. [4]Carnegie Institution of Washington, Geophysical Laboratory, 5251 Broad Branch Road N.W., Washington, DC 20018, USA.

*To whom correspondence should be addressed. E-mail: schweitzer@ncsu.edu

†Present address: Department of Geosciences, Christian-Albrechts University Kiel, Olshausenstrasse 40, 24098 Kiel, Germany.

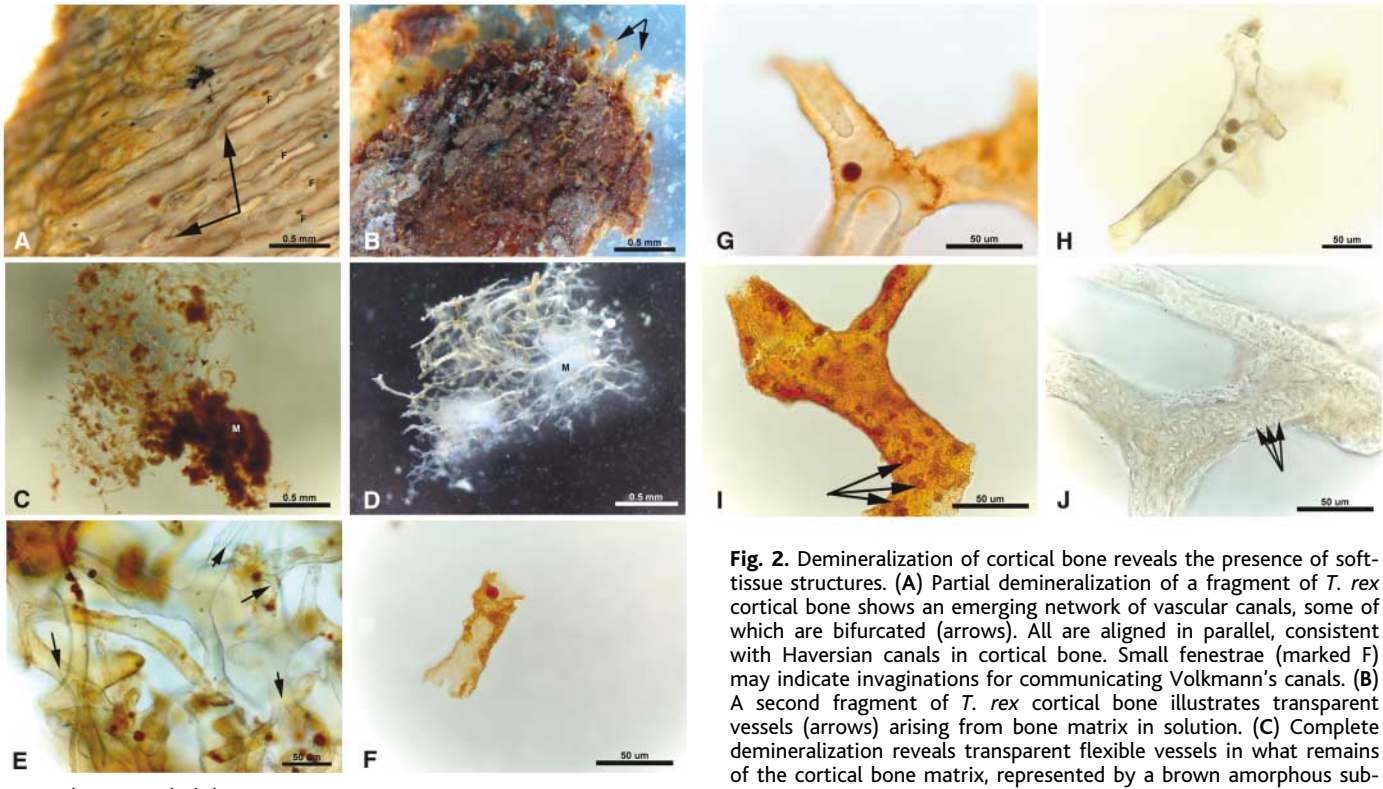

Fig. 2. Demineralization of cortical bone reveals the presence of soft-tissue structures. (**A**) Partial demineralization of a fragment of *T. rex* cortical bone shows an emerging network of vascular canals, some of which are bifurcated (arrows). All are aligned in parallel, consistent with Haversian canals in cortical bone. Small fenestrae (marked F) may indicate invaginations for communicating Volkmann's canals. (**B**) A second fragment of *T. rex* cortical bone illustrates transparent vessels (arrows) arising from bone matrix in solution. (**C**) Complete demineralization reveals transparent flexible vessels in what remains of the cortical bone matrix, represented by a brown amorphous substance (marked M). (**D**) Ostrich vessel after demineralization of cortical bone and subsequent digestion of fibrous collagenous matrix. Transparent vessels branch and remain associated with small regions of undigested bone matrix, seen here as amorphous, white fibrous material (marked M). Scale bars in (A) to (D), 0.5 mm. (**E**) Higher magnification of dinosaur vessels shows branching pattern (arrows) and internal contents. Vascular structure is not consistent with fungal hyphae (no septae, and branching pattern is not consistent with fungal morphology) or plant (no cell walls visible, and again branching pattern is not consistent). Round red microstructures within the vessels are clearly visible. (**F**) *T. rex* vessel fragment, containing microstructures consistent in size and shape with those seen in the ostrich vessel in (H). (**G**) Second fragment of dinosaur vessel. Air/fluid interfaces, represented by dark menisci, illustrate the hollow nature of vessels. Microstructure is visible within the vessel. (**H**) Ostrich vessel digested from demineralized cortical bone. Red blood cells can be seen inside the branching vessel. (**I**) *T. rex* vessel fragment showing detail of branching pattern and structures morphologically consistent with endothelial cell nuclei (arrows) in vessel wall. (**J**) Ostrich blood vessel liberated from demineralized bone after treatment with collagenase shows branching pattern and clearly visible endothelial nuclei. Scale bars in (E) to (J), 50 μm. (F), (I), and (J) were subjected to aldehyde fixation (*3*). The remaining vessels are unfixed.

after 7 days, several fragments of the lining tissue exhibited unusual characteristics not normally observed in fossil bone. Removal of the mineral phase left a flexible vascular tissue that demonstrated great elasticity and resilience upon manipulation. In some cases, repeated stretching was possible (Fig. 1A, arrow), and small pieces of this demineralized bone tissue could undergo repeated dehydration-rehydration cycles (Fig. 1B) and still retain this elastic character. Demineralization also revealed that some regions of the bone were highly fibrous (Fig. 1C, arrows).

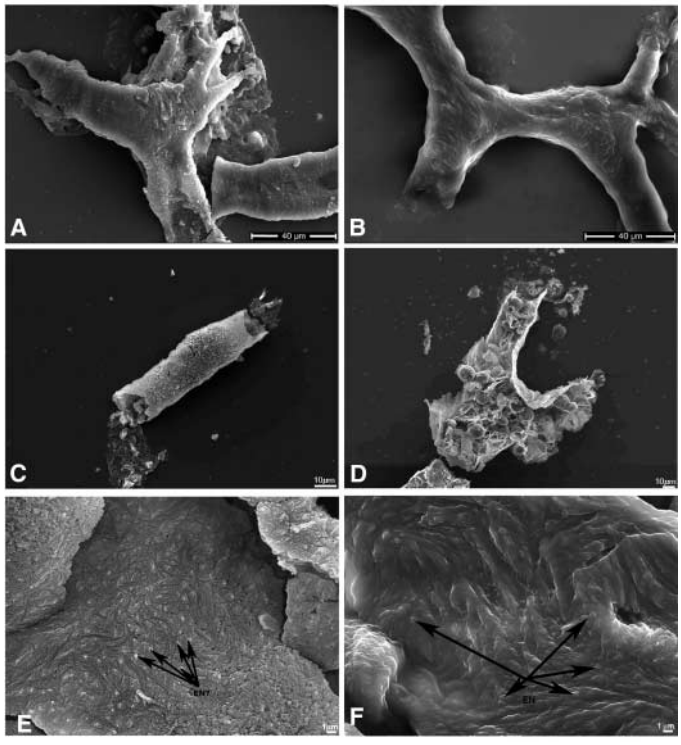

Fig. 3. SEM images of aldehyde-fixed vessels. (**A**) Isolated vessel from *T. rex*. (**B**) Vessel isolated from extant ostrich after demineralization and collagenase digestion (*3*). (**C**) Vessel from *T. rex*, showing internal contents and hollow character. (**D**) Exploded *T. rex* vessel showing small round microstructures partially embedded in internal vessel walls. (**E**) Higher magnification of a portion of *T. rex* vessel wall, showing hypothesized endothelial nuclei (EN). (**F**) Similar structures visible on fixed ostrich vessel. Striations are seen in both (E) and (F) that may represent endothelial cell junctions or alternatively may be artifacts of the fixation/dehydration process. Scale bars in (A) and (B), 40 μm; in (C) and (D), 10 μm; in (E) and (F), 1 μm.

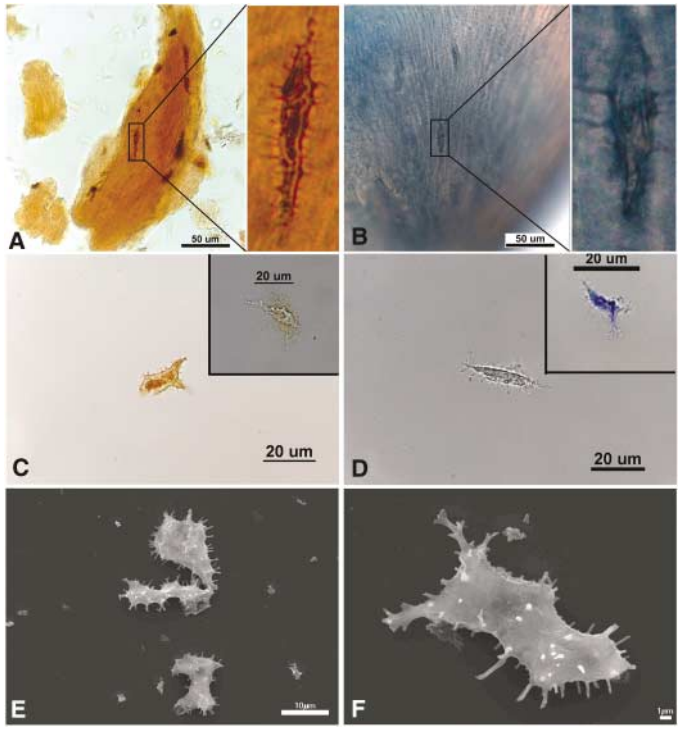

Fig. 4. Cellular features associated with *T. rex* and ostrich tissues. (**A**) Fragment of demineralized cortical bone from *T. rex*, showing parallel-oriented fibers and cell-like microstructures among the fibers. The inset is a higher magnification of one of the microstructures seen embedded in the fibrous material. (**B**) Demineralized and stained (*3*) ostrich cortical bone, showing fibrillar, parallel-oriented collagen matrix with osteocytes embedded among the fibers. The inset shows a higher magnification of one of the osteocytes. Both inset views show elongate bodies with multiple projections arising from the external surface consistent with filipodia. (**C**) Isolated microstructure from *T. rex* after fixation. In addition to the multiple filipodial-like projections, internal contents can be seen. The inset shows a second structure with long filipodia and an internal transparent nucleus-like structure. (**D**) Fixed ostrich osteocyte; inset, ostrich osteocyte fixed and stained for better visualization. Internal contents are discernible, and filipodia can be seen extending in multiple planes from the cell surface. (**E** and **F**) SEM images of aldehyde-fixed (*3*) microstructures isolated from *T. rex* cortical bone tissues. Scale bars in (A) and (B), 50 μm; in (C) and (D), 20 μm; in (E), 10 μm; in (F), 1 μm.

Partial demineralization of the cortical bone revealed parallel-oriented vascular canals that were seen to bifurcate in some areas (Fig. 2A, arrows). Occasional fenestrae (marked F) were observed on the surface of the vascular canals, possibly correlating with communicating Volkmann's canals. Complete demineralization of the cortical bone released thin and transparent soft-tissue vessels from some regions of the matrix (Fig. 2, B and C), which floated freely in the demineralizing solution. Vessels similar in diameter and texture were recovered from extant ostrich bone, when demineralization was followed by digestion with collagenase enzyme (*3*) to remove densely fibrous collagen matrix (Fig. 2D). In both dinosaur (Fig. 2C) and ostrich (Fig. 2D), remnants of the original organic matrix in which the vessels were embedded can still be visualized under transmitted light microscopy. These vessels are flexible, pliable, and translucent (Fig. 2E). The vessels branch in a pattern consistent with extant vessels, and many bifurcation points are visible (Fig. 2E, arrows). Many of the dinosaur vessels contain small round microstructures that vary from deep red to dark brown (Fig. 2, F and G). The vessels and contents are similar in all respects to blood vessels recovered from extant ostrich bone (Fig. 2H). Aldehyde-fixed (*3*) dinosaur vessels (Fig. 2I) are virtually identical in overall morphology to similarly prepared ostrich vessels (Fig. 2J), and structures consistent with remnants of nuclei from the original endothelial cells are visible on the exterior of both dinosaur and ostrich specimens (Fig. 2, I and J, arrows).

Under scanning electron microscopy (SEM) (Fig. 3), features seen on the external surface of dinosaurian vessels are virtually indistinguishable from those seen in similarly prepared extant ostrich vessels (Fig. 3, B and F), suggesting a common origin. These features include surface striations that may be consistent with endothelial cell junctions, or alternatively may be artifacts of fixation and/or dehydration. In addition, small round to oval features dot the surface of both dinosaur and ostrich vessels, which may be consistent with endothelial cell nuclei (Fig. 3, E and F, arrows).

Finally, in those regions of the bone where fibrillar matrix predominated in the demineralized tissues, elongate microstructures could be visualized among the fibers (Fig. 4A, inset). These microstructures contain multiple projections on the external surface and are virtually identical in size, location, and overall morphology to osteocytes seen among colla-

gen fibers of demineralized ostrich bone (Fig. 4B, inset). These cell-like microstructures could be isolated and, when subjected to aldehyde fixation (*3*), appeared to possess internal contents (Fig. 4C), including possible nuclei (Fig. 4C, inset). These microstructures are similar in morphology to fixed ostrich osteocytes, both unstained (Fig. 4D) and stained (*3*) for better visualization (Fig. 4D, inset). SEM verifies the presence of the features seen in transmitted light microscopy, and again, projections extending from the surface of the microstructures are clearly visible (Fig. 4, E and F).

The fossil record is capable of exceptional preservation, including feathers (*4*–*6*), hair (*7*), color or color patterns (*7*, *8*), embryonic soft tissues (*9*), muscle tissue and/or internal organs (*10*–*13*), and cellular structure (*7*, *14*–*16*). These soft tissues are preserved as carbon films (*4*, *5*, *10*) or as permineralized three-dimensional replications (*9*, *11*, *13*), but in none of these cases are they described as still-soft, pliable tissues.

Mesozoic fossils, particularly dinosaur fossils, are known to be extremely well preserved histologically and occasionally retain molecular information (*6*, *17*, *18*), the presence of which is closely linked to morphological preservation (*19*). Vascular microstructures that may be derived from original blood materials of Cretaceous organisms have also been reported (*14*–*16*).

Pawlicki was able to demonstrate osteocytes and vessels obtained from dinosaur bone using an etching and replication technique (*14*, *15*). However, we demonstrate the retention of pliable soft-tissue blood vessels with contents that are capable of being liberated from the bone matrix, while still retaining their flexibility, resilience, original hollow nature, and three-dimensionality. Additionally, we can isolate three-dimensional osteocytes with internal cellular contents and intact, supple filipodia that float freely in solution. This *T. rex* also contains flexible and fibrillar bone matrices that retain elasticity. The unusual preservation of the originally organic matrix may be due in part to the dense mineralization of dinosaur bone, because a certain portion of the organic matrix within extant bone is intracrystalline and therefore extremely resistant to degradation (*20*, *21*). These factors, combined with as yet undetermined geochemical and environmental factors, presumably also contribute to the preservation of soft-tissue vessels. Because they have not been embedded or subjected to other chemical treatments, the cells and vessels are capable of being analyzed further for the persistence of molecular or other chemical information (*3*).

Using the methodologies described here, we isolated translucent vessels from two other exceptionally well-preserved tyrannosaurs (figs. S1 and S2) (*3*), and we isolated microstructures consistent with osteocytes in at least three other dinosaurs: two tyrannosaurs and one hadrosaur (fig. S3). Vessels in these specimens exhibit highly variable preservation, from crystalline morphs to transparent and pliable soft tissues.

The elucidation and modeling of processes resulting in soft-tissue preservation may form the basis for an avenue of research into the recovery and characterization of similar structures in other specimens, paving the way for micro- and molecular taphonomic investigations. Whether preservation is strictly morphological and the result of some kind of unknown geochemical replacement process or whether it extends to the subcellular and molecular levels is uncertain. However, we have identified protein fragments in extracted bone samples, some of which retain slight antigenicity (*3*). These data indicate that exceptional morphological preservation in some dinosaurian specimens may extend to the cellular level or beyond. If so, in addition to providing independent means of testing phylogenetic hypotheses about dinosaurs, applying molecular and analytical methods to well-preserved dinosaur specimens has important implications for elucidating preservational microenvironments and will contribute to our understanding of biogeochemical interactions at the microscopic and molecular levels that lead to fossilization.

References and Notes

1. J. R. Horner, K. Padian, *Proc. R. Soc. London Ser. B* **271**, 1875 (2004).
2. M. Schweitzer, J. L. Wittmeyer, J. R. Horner, in preparation.
3. Materials and methods are available as supporting material on *Science* Online.
4. X. Xu, X. L. Wang, X. C. Wu, *Nature* **401**, 262 (1999).
5. Q. Ji *et al.*, *Nature* **393**, 753 (1998).
6. M. H. Schweitzer *et al.*, *J. Exp. Zool.* **285**, 146 (1999).
7. M. Wuttke, in *Messel–Ein Schaufenster in die Geschichte der Erde und des Lebens*, S. Schaal, W. Ziegler, Eds. (Verlag Waldemar Kramer, Frankfurt am Main, Germany, 1988), pp. 265–274.
8. D. M. Martill, E. Frey, *N. Jb. Geol. Paläont. Mh.* **2**, 118 (1995).
9. L. M. Chiappe *et al.*, *Nature* **396**, 258 (1998).
10. C. Dal Sasso, M. Signore, *Nature* **392**, 383 (1998).
11. A. W. A. Kellner, *Nature* **379**, 32 (1996).
12. N. L. Murphy, D. Trexler, M. Thompson, *J. Vertebr. Paleontol.* **33**, 91A (2002).
13. D. E. G. Briggs, P. R. Wilby, B. P. Perez-Moreno, J. L. Sanz, M. Fregenal-Martinez, *J. Geol. Soc. (London)* **154**, 587 (1997).
14. R. Pawlicki, A. Korbel, H. Kubiak, *Nature* **211**, 656 (1966).
15. R. Pawliki, M. Nowogrodzka-Zagorska, *Ann. Anat.* **180**, 73 (1998).
16. M. H. Schweitzer, J. R. Horner, *Ann. Paleontol.* **85**, 179 (1999).
17. G. Muyzer *et al.*, *Geology* **20**, 871 (1992).
18. M. H. Schweitzer *et al.*, *Proc. Natl. Acad. Sci. U.S.A.* **94**, 6291 (1997).
19. R. E. M. Hedges, *Archaeometry* **44**, 319 (2002).
20. S. Weiner, W. Traub, H. Elster, M. J. DeNiro, *Appl. Geochem.* **4**, 231 (1989).
21. G. A. Sykes, M. J. Collins, D. I. Walton, *Org. Geochem.* **23**, 1059 (1995).

22. We thank C. Ancell, J. Barnes, D. Enlow, J. Flight, B. Harmon, E. Lamm, N. Myrhvold, A. de Ricqles, and A. Steele for funding, preparation, insight, consultation, and valued feedback; and J. Fountain and K. Padian for editorial advice. Research was funded by North Carolina State University as well as by grants from N. Myhrvold (J.R.H.) and NSF (M.H.S.).

Supporting Online Material

www.sciencemag.org/cgi/content/full/307/5717/1952/DC1
Materials and Methods
Figs. S1 to S5
References

7 December 2004; accepted 26 January 2005
10.1126/science.1108397

Glycan Foraging in Vivo by an Intestine-Adapted Bacterial Symbiont

Justin L. Sonnenburg,[1,2] Jian Xu,[1,2] Douglas D. Leip,[1,2] Chien-Huan Chen,[1,2] Benjamin P. Westover,[1,3] Jeremy Weatherford,[3] Jeremy D. Buhler,[1,3] Jeffrey I. Gordon[1,2]*

Germ-free mice were maintained on polysaccharide-rich or simple-sugar diets and colonized for 10 days with an organism also found in human guts, *Bacteroides thetaiotaomicron*, followed by whole-genome transcriptional profiling of bacteria and mass spectrometry of cecal glycans. We found that these bacteria assembled on food particles and mucus, selectively induced outer-membrane polysaccharide-binding proteins and glycoside hydrolases, prioritized the consumption of liberated hexose sugars, and revealed a capacity to turn to host mucus glycans when polysaccharides were absent from the diet. This flexible foraging behavior should contribute to ecosystem stability and functional diversity.

The adult human body is a composite of many species. Each of us harbors ~10 times as many microbial cells as human cells (*1*). Our resident microbial communities provide us with a variety of metabolic capabilities not encoded in our genome, including the ability to harvest otherwise inaccessible nutrients from our diet (*2*). The intestine contains an estimated 10 trillion to 100 trillion microorganisms that are largely members of Bacteria but include representatives from